Analysis of Undersea Simultaneous Wireless Power and 1 Mb/s Data Rate Transfer System Based on DDQ Coil

Chaolai Da, Lifang Wang, *Member, IEEE*, Fang Li, Chengxuan Tao, *Member, IEEE*, and Yuwang Zhang

***Abstract*—This article proposed an undersea simultaneous wireless power and data transfer system. It can achieve 1 Mb/s communication rate for autonomous underwater vehicles. DDQ coil was used to design an integrated magnetic coupling mechanism that decoupled the power channel from the data channel. In order to obtain 1 Mb/s communication rate in seawater, the frequency characteristics and eddy current loss of DDQ coil in seawater are studied. By establishing the steady-state and dynamic models of the data channel, the data gain and dynamic response time (DRT) of the amplitude shift keying modulation are accurately calculated. The influences of the parameters on data gain and DRT are analyzed in seawater, and the design procedure of system parameters is proposed. Finally, a 884 W prototype in seawater is built. The power transfer efficiency of the prototype is 94.3%, and the communication rate is up to 1 Mb/s. The experimental results prove the correctness of the theoretical analysis in this article.**

***Index Terms*—Dynamic response time (DRT), eddy current, simultaneous wireless power and data transfer (SWPDT), undersea wireless power transfer (UWPT).**

I. Introduction

In RECENT years, wireless power transfer (WPT) has been widely applied in electric vehicles [1], [2], [3], implantable medical devices [4], consumer electronics [5], and autonomous underwater vehicles (AUVs) due to its safety and convenience [6].

In order to eliminate safety issues like line loss and wet plugging in seawater, the AUV can be charged via the WPT technology [7], [8]. At present, many research institutions have conducted a lot of research on undersea wireless power transfer (UWPT), including magnetic coupling mechanism design [9], [10], eddy current loss analysis [11], and parameter optimization [12]. Meanwhile, AUV must establish real-time and reliable communication between the power supply and itself to ensure stable operation. Hydroacoustic, optical, and electromagnetic communication can be used to establish communication between electrical equipment working in seawater [13]. Hydroacoustic communication has a low rate, and optical communication is poorly concealed, which leads to the fact that they are unsuitable in the UWPT system. Therefore, this article focuses on electromagnetic communication.

Electromagnetic communication usually has some methods, such as Wi-Fi, Bluetooth, and ZigBee. However, when these technologies are applied in the UWPT system, there are some problems, such as low signal-to-noise ratio (SNR), high delay time, and attenuation [14], [15], [16], [17]. Simultaneous wireless power and data transfer (SWPDT) is an optimal way to obtain a high communication rate and SNR during high-power transmission [18], [19]. However, there is a relative lack of work on SWPDT in seawater. Therefore, this article studies the application of SWPDT in seawater based on existing research findings.

Although there are relatively few references for undersea simultaneous wireless power and data transfer (USWPDT), the research findings of SWPDT in air have significant reference value for the design of the USWPDT system [20], [21], [22], [23], [24], [25], [26].

SWPDT system usually uses the same pair of coils or two independent pairs of coils to transfer power and data synchronously. Li et al. [20] used unipolar coils to transfer power, while series-connected perpendicular bipolar coils were used for data transfer. The transfer efficiency reached 87%, and the communication rate was 19.2 kb/s. Wei et al. [21] used a double-D coil to deliver power and data efficiently, in which the data was injected into one of the D coils. The transfer efficiency reached 90%, and the communication rate was 166.7 kb/s. Yao et al. [22] used a pair of coupling coils with taps to synchronize wireless power and data transfer. The power transmitted by the SWPDT system was 300 W, and the full duplex communication rate was 500 kb/s. Regrettably, whether using the same pair of coils or two independent pairs of coils, the crosstalk between

Manuscript received 28 February 2023; revised 29 May 2023; accepted 19 June 2023. Date of publication 28 June 2023; date of current version 1 September 2023. This work was supported by the National Key R&D Program of China under Grant 2021YFC2800201. Recommended for publication by Associate Editor M. Amirabadi. *(Corresponding author: Fang Li.)*

Chaolai Da, Lifang Wang, Fang Li, and Yuwang Zhang are with the Key Laboratory of Power Electronics and Electric Drives, Institute of Electrical Engineering, Chinese Academy of Sciences, Beijing 100190, China, and also with the University of Chinese Academy of Sciences, Beijing 100049, China (e-mail: dachaolai@mail.iee.ac.cn; wlf@mail.iee.ac.cn; lifang@mail.iee.ac.cn; zhangyuwang@mail.iee.ac.cn).

Chengxuan Tao is with the School of Mechanical Engineering, Beijing Institute of Technology, Beijing 100081, China, also with the Key Laboratory of Power Electronics and Electric Drives, Institute of Electrical Engineering, Chinese Academy of Sciences, Beijing 100190, China, and also with the University of Chinese Academy of Sciences, Beijing 100049, China (e-mail: taochengxuan@mail.iee.ac.cn).

Color versions of one or more figures in this article are available at https://doi.org/10.1109/TPEL.2023.3290162.

Digital Object Identifier 10.1109/TPEL.2023.3290162

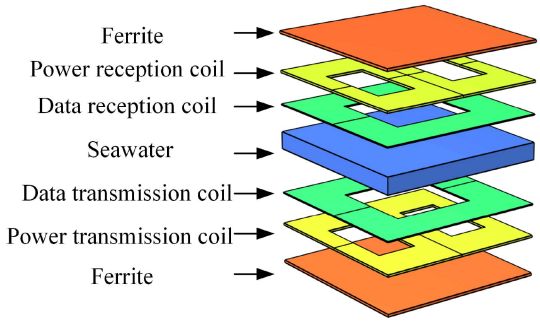

Fig. 1. Schematic diagram of magnetic coupling mechanism of USWPDT system.

the power and data channels cannot be suppressed entirely due to electromagnetic interference (EMI).

The topology design is critical in the SWPDT system. In [23], a dual-channel transfer model was constructed for integrating bidirectional data communication into a WPT system based on a single-coil, dual-resonant structure. In [24], a novel SWPDT system based on the double-side *LCCL* and dual-notch filter was proposed to solve the interference between the power and data. Fan et al. [25] proposed a double-side *LCC* compensation topology for power transfer, while a four resonance dual-rejection structure constituted the data transfer channel. The SWPDT system was presented in [26] based on double-sided inductor–capacitor–capacitor compensation topology and frequency-shift keying. SNR of the system was 47 dB, and the communication rate was 150 kb/s. However, all of the abovementioned topologies are complex and add difficulty to the design of the system parameters in the seawater environment. The two reasons are as follows.

On the one hand, the eddy current loss from MHz-class signal excitation is very substantial, and increases the equivalent internal resistance of the coil; on the other hand, the eddy current field in the seawater impacts the original flux distribution of the coil. These two factors cause the impedance value of the data channel to vary in several of ways depending on the coil's winding direction, transmission distance, and parasitic characteristics. When the single-coil, dual-resonant structure proposed in [23] is used in seawater, the communication quality will be degraded because the variation of internal resistance and flux will cause the resonance point to be offset. The data channels in [24] and [25] use several passive components and power coil to transfer data, both of which result in communication systems cannot reach Mb/s-class communication rate in seawater due to their excessively long dynamic response time (DRT) and high eddy current equivalent internal resistance. The power coil is also used in [26] to transfer data, but it is unable to increase the carrier frequency due to the large parasitic capacitance and eddy current loss equivalent internal resistance, which prevents it from achieving Mb/s-class communication rate.

For the USWPDT system, Yang et al. [13], Wang et al. [16], and Zeng et al. [27] proposed the application of the SWPDT system in seawater. Nevertheless, the operating characteristics of the USWPDT system were not analyzed in detail in [13], and the frequency characteristics of the coil in seawater due to the effect of conductivity were not analyzed in [16]. A SWPDT system based on a novel multidirectional magnetic coupler is proposed for the application of swarm AUVs in [27]. Although the system can achieve 92.25% efficiency at a power level of 200 W when four AUVs are powered, the communication rate is only 30 kb/s.

In addition, the dynamic response of the data channel is an essential factor in constraining the communication rate if the amplitude shift keying (ASK) modulation is used. However, the current research utilizes the estimation method and does not accurately establish the dynamic response model of ASK data to calculate its DRT.

In order to achieve Mb/s-class communication rate as well as relatively high-power transfer, this article proposes a USWPDT system based on the DDQ coil. First, guidelines for the establishment of data channel are provided by the analysis of the frequency properties of DDQ coil in seawater in Section II. Next, the steady-state data model and the dynamic response model based on ASK modulation are accurately constructed and analyzed in Section III. Finally, the communication rate of the proposed USWPDT system is up to 1 Mb/s when the output power is 884 W in Section IV. Finally, Section V concludes this article. The main innovations and contributions of this article are summarized as follows.

1) DDQ coil realizes the decoupling between the power channel and communication channel in this article. By analyzing the frequency characteristics of the DDQ coil in seawater, a method to establish a communication system in seawater is proposed.
2) To maximize the communication rate when the carrier frequency is not increased, this article analyzes the relationship between the system parameters and the DRT of ASK modulation. Also, combining the steady-state and dynamic model of ASK modulation, an overall parameter optimization of the communication channel can be performed for a given condition.
3) The experimental prototype presented in this article achieves Mb/s-class communication rate under a relatively high-power level, which can provide a practical method for SWPDT system. In addition, the theoretical analysis in this article can guide the design of SWPDT system in the special seawater environment.

II. Frequency Characteristic of DDQ Coil

In the proposed SWPDT system, a pair of DD coils are used to transfer power, and a pair of rectangular coils(Q coils) are used to transfer data. As shown in Fig. 1, DD coils and Q coils are decoupled. The theoretical cross-coupling coefficient between the power channel and data channel is 0.

In principle, the frequency of the data carrier needs to be lower than the self-resonant frequency of the coil. A data coil with a high self-resonant frequency can inject a high frequency data carrier to obtain a rapid communication rate. However, the inherent parasitic capacitance of the coil causes it to have a low self-resonant frequency, which utmostly reduces the communication rate. At the same time, the eddy current field generated

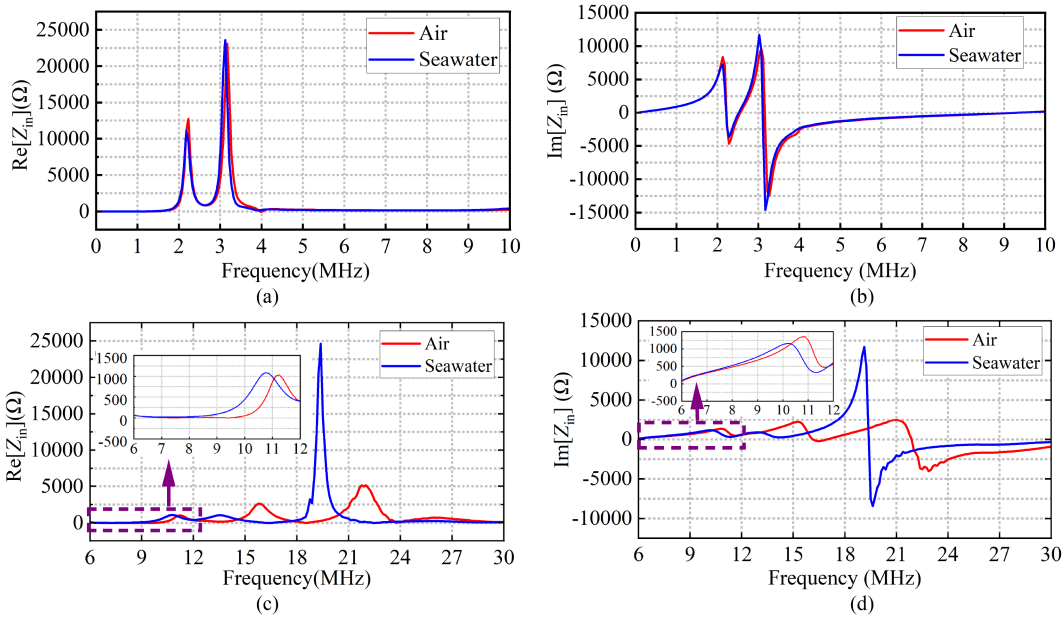

Fig. 2. Input impedance of DDQ coil. (a) Real part of the input impedance of DD coil. (b) Imaginary part of the input impedance of DD coil. (c) Real part of the input impedance of Q coil. (d) Imaginary part of the input impedance of Q coil.

by the seawater conductivity has an effect on the internal resistance and flux distribution of the coil, which in turn affects its self-resonant frequency.

In this article, as shown in Fig. 2, the input impedance of DDQ coil was measured in air and seawater using a network analyzer E5061B. When the excitation frequency is lower than the self-resonant frequency of the coil, the real part of the input impedance can represent the changing trend of the internal resistance of the coil, and the imaginary part of the input impedance can describe the changing trend of the inductance of the coil.

Fig. 2(a) and (b) present the measurement results of the real and imaginary parts of the input impedance of the DD coil. Compared to the Q-coil, which transmits the data, the DD coil has greater self-inductance and consists of two unipolar coils connected in reverse series. Consequently, there are three lower self-resonant frequency points in Fig. 2(b) that result in the imaginary part of the input impedance being zero. The seawater has minimal effect on the three self-resonant frequency points of the DD coil.

Fig. 2(c) and (d) present the measurement results of the real and imaginary parts of the input impedance of the Q coil. The self-resonant frequency of the Q coil exceeds 21 MHz in air, but it is notably lower in seawater. When the frequency is higher than 9 MHz, the internal resistance and self-inductance of the Q coil are susceptible to frequency, which is not conducive to the design of the data circuit. Therefore, the carrier frequency of the data should be set below 9 MHz to obtain better communication performance. In this article, the carrier frequency is 8 MHz. In addition, it is worth noting that the other resonance peaks below the highest resonance peak in Fig. 2(c) and (d) are due to interference from other coils. The crosstalk generated by them can be coupled into the data channel to interfere with communication performance.

III. Characteristics of the SWPDT System

The equivalent circuit of the proposed USWPDT system is shown in Fig. 3. $U_{\rm in}$ and $I_{\rm in}$ are the dc voltage source voltage and output current, respectively. $C_{\rm in}$ is the primary inverter input capacitor; meanwhile, $U_{\rm L}$ and $I_{\rm L}$ are the voltage and current of the load, respectively.

$R_{\rm L}$ is the equivalent load resistance of the AUV energy storage battery during charging. $C_{\rm out}$ is the secondary dc filter capacitor. Four power electronic switches Q_1–Q_4 form the primary full-bridge inverter. $u_{\rm inv}$ and $i_{\rm inv}$ are its output voltage and output current. Four diodes D_1–D_4 form the secondary full-bridge rectifier. $u_{\rm rec}$ and $i_{\rm rec}$ are its input voltage and input current, respectively. $L_{\rm p1}(L_{\rm p2})$ is the primary (secondary) side compensation inductor. $C_{\rm p1}(C_{\rm p2})$ is the primary (secondary) side parallel compensation capacitor, and $C_{\rm pp}(C_{\rm ps})$ is the primary (secondary) side series compensation capacitor, which forms the *LCC/LCC* compensation network. Due to the fact that $L_{\rm p1}$ and $L_{\rm p2}$ are placed in the pressure-resistant compartment without eddy current loss in UWPT system, and they have a small internal resistance compared to power coil in air. Therefore, their internal resistance is ignored in this article.

In addition, $L_{\rm pp}(L_{\rm ps})$ is the primary (secondary) side power transfer coil with internal resistance $R_{\rm pp}(R_{\rm ps})$, and $i_{\rm pp}(i_{\rm ps})$ is the current flowing through it. $L_{\rm sp}(L_{\rm ss})$ is the primary (secondary) side data transfer coil with internal resistance $R_{\rm sp}(R_{\rm ss})$, and $i_{\rm sp}(i_{\rm ss})$ is the current flowing through it. $k_{\rm power}$ is the coupling coefficient between the two power transfer coils, and $k_{\rm signal}$ is the coupling coefficient between the two data transfer coils. $C_{\rm sp}(C_{\rm ss})$ is the primary (secondary) side data transfer compensation capacitor. $u_{\rm in\_signal}$ is the equivalent power amplifier at the data transmitting port, and $R_{\rm signal}$ is the sampling resistor at the data receiving port. The voltage of $R_{\rm signal}$ is $u_{\rm out\_signal}$. The

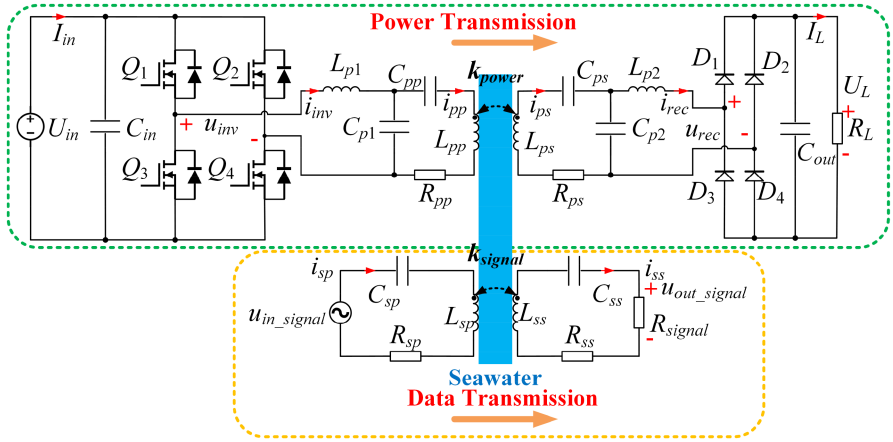

Fig. 3. Equivalent circuit diagram of the proposed USWPDT system.

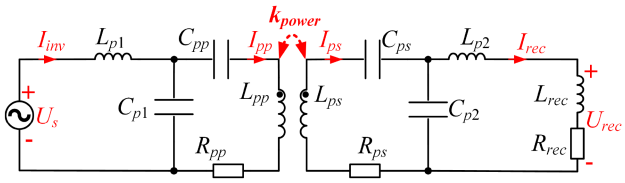

Fig. 4. Equivalent circuit of UWPT system.

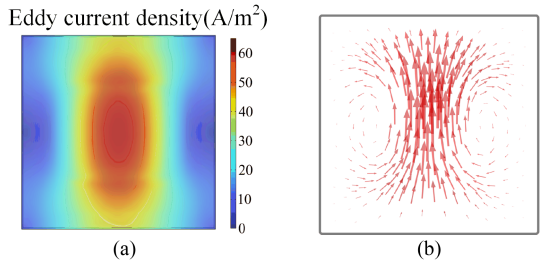

Fig. 5. Eddy current loss distribution of DD coil. (a) Eddy current density distribution of DD coil. (b) Eddy current vector distribution of DD coil.

design principle of WPT in this article is the same as that of the conventional *LCC/LCC* topology. The data transfer circuit uses the SS compensation topology.

A. Power Transfer Analysis

The power transfer circuit in Fig. 3 can be simplified to the equivalent circuit shown in Fig. 4. Where $U_{\rm s}$ is the root mean square value of $u_{\rm inv}$ with frequency $f_{\rm p}$, $\omega_{\rm p} = 2\pi f_{\rm p}$. Due to the nonlinear characteristics of the rectifier, its input impedance can be equated to a series connection of a resistor $R_{\rm rec}$ and an inductor $L_{\rm rec}$ [3]. $U_{\rm rec}$ is the root mean square value of $u_{\rm rec}$, there $U_s = 2\sqrt{2}U_{\rm in}/\pi$,$U_{rec} = 2\sqrt{2}U_L/\pi$.

$I_{\rm inv}$, $I_{\rm pp}$, $I_{\rm ps}$, and $I_{\rm rec}$ are the root mean square values of $i_{\rm inv}$, $i_{\rm pp}$, $i_{\rm ps}$, and $i_{\rm rec}$, respectively. $k_{\rm power}$ is the coupling coefficient between the two power transfer coils, $k_{\rm power} = M_p/\sqrt{L_{pp}L_{ps}}$. To ensure that the WPT system operates in a resonant state, the *LCC/LCC* compensation network needs to meet the following conditions:

$$\begin{cases} \omega_p L_{p1} = 1/\left(\omega_p C_{p1}\right), \omega_p L_{p2} = 1/\left(\omega_p C_{p2}\right) \\ \omega_p L_{pp} = 1/\left(\omega_p C_{pp}\right) + 1/\left(\omega_p C_{p1}\right) \\ \omega_p L_{ps} = 1/\left(\omega_p C_{ps}\right) + 1/\left(\omega_p C_{p2}\right). \end{cases} \tag{1}$$

Solving the KVL equation, the output power can be derived

$$P_{\rm out} = \left| \left(\frac{-j\omega_p M_p L_{p2} U_s}{\left(\left(\mathrm{j}\omega_p L_{rec} + R_{rec}\right) R_{ps} + \omega_p^2 L_{p2}^2\right) L_{p1}} \right)^2 \times \left(\mathrm{j}\omega_p L_{rec} + R_{rec}\right) \right|. \tag{2}$$

The transfer efficiency is

$$\eta_p = \left| \frac{\omega_p^2 L_{p2}^2}{A + R_{pp} L_{p1}^2 A^2 / B} \right|. \tag{3}$$

Among them

$$\begin{cases} A = \left(\mathrm{j}\omega_p L_{rec} + R_{rec}\right) R_{ps} + \omega_p^2 L_{p2}^2 \\ B = \left(\mathrm{j}\omega_p L_{rec} + R_{rec}\right) \omega_p^2 M_p^2 L_{p1}^2. \end{cases} \tag{4}$$

Here, $R_{\rm pp}$ and $R_{\rm ps}$ are the equivalent internal resistance of $L_{\rm pp}$ and $L_{\rm ps}$, respectively, which can be expressed as

$$\begin{cases} R_{pp} = R_{pp\_\rm ac} + R_{pp\_\rm eddy} \\ R_{ps} = R_{ps\_\rm ac} + R_{ps\_\rm eddy} \end{cases}. \tag{5}$$

In the abovementioned equation, $R_{\rm pp\_ac}(R_{\rm ps\_ac})$ is the ac internal resistance introduced by $L_{\rm pp}(L_{\rm ps})$, and $R_{\rm pp\_eddy}(R_{\rm ps\_eddy})$ is the equivalent internal resistance due to eddy current loss generated by $L_{\rm pp}(L_{\rm ps})$ in seawater [11]. Because $R_{\rm pp}$ and $R_{\rm ps}$ contain $R_{\rm pp\_eddy}$ and $R_{\rm ps\_eddy}$ of eddy current loss caused by the system working in seawater, the power transfer is affected by $R_{\rm pp\_eddy}$, $R_{\rm ps\_eddy}$, and $M_{\rm p}$.

Referring to [11], the equivalent internal resistance $R_{\rm pp\_eddy}(R_{\rm ps\_eddy})$ introduced by the coil due to eddy current losses is calculated by the finite element method in the initial stage of the system design. In this article, finite element analysis of the eddy current losses of the coil was carried out by COMSOL. Fig. 5 shows the distribution of eddy current losses

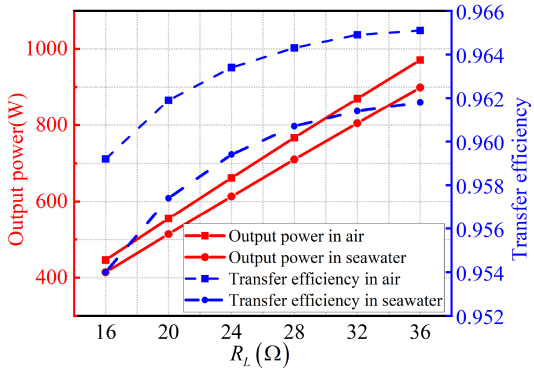

Fig. 6. Comparison of output power and transfer efficiency in air and seawater.

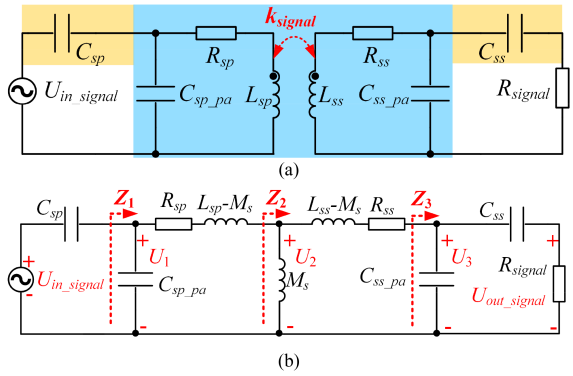

Fig. 7. Data transfer circuit model. (a) Data transfer equivalent circuit. (b) Data transfer T-equivalent circuit.

TABLE I
PARAMETER VALUES OF THE PROTOTYPE

Parameters	Values
L_{pp}, L_{ps}, L_{sp}, L_{ss} (μH)	120.7, 131.3, 15.1, 14.4
M_p, M_s in air(μH)	42.1, 7.8
M_p, M_s in seawater(μH)	40.5, 7.7
L_{p1}, L_{p2}(μH)	49.1,48.8
R_{pp}, R_{ps}, R_{sp}, R_{ss} in air(Ω)	0.17, 0.18, 7.85, 6.98
R_{pp}, R_{ps}, R_{sp}, R_{ss} in seawater(Ω)	0.20, 0.21, 28.61, 32.71
C_{p1}, C_{p2}, C_{pp}, C_{ps}(nF)	72.4, 71.7, 48.1, 41.4,
C_{sp}, C_{ss}, C_{sp_pa}, C_{ss_pa}(pF)	20, 20, 3.5, 3.4
U_{in}, U_{in_signal}	200 V, 15 V
R_L, R_{signal}	36 Ω, 1200 Ω
f_p, f_s	85 kHz, 8 MHz
Q_{pp}, Q_{ps}, Q_{sp}, Q_{ss} in air	379.2, 389.6, 96.7, 103.7
Q_{pp}, Q_{ps}, Q_{sp}, Q_{ss} in seawater	322.3, 333.9, 26.5, 22.1
Conductivity of seawater	3.6 S/m
Number of turns of DD coil	15
Number of turns of Q coil	8

in the DD coil at $f_p = 85$ kHz for 1 A current excitation, which is mainly distributed at the adjacent position of two unipolar coils.

From (2)–(5), it is clear that R_{pp_eddy}, R_{ps_eddy}, and M_p affect the output power and efficiency of the UWPT system. Fig. 6 compares output power and transfer efficiency at different R_L in air and seawater, which involves the parameters shown in Table I. Since the *LCC/LCC* topology has a constant current output characteristic, the output power increases linearly with increasing R_L. The output power in air is greater than that in seawater. Meanwhile, the transfer efficiency rises slowly with the increase of R_L, and the transfer efficiency in air is greater than in seawater.

B. Data Transfer Steady Analysis

The data transfer circuit in Fig. 3 can be simplified to the equivalent circuit shown in Fig. 7(a). Where k_{signal} is the coupling coefficient between the two data transmission coils $k_{signal} = M_s/\sqrt{L_{sp}L_{ss}}$. The blue part represents the inherent parameters of the Q coil, and the orange part represents the SS compensation network of the data circuit. R_{sp} and R_{ss} are the equivalent internal resistance of L_{sp} and L_{ss}, respectively, which can be expressed as

$$\begin{cases} R_{sp} = R_{sp\_ac} + R_{sp\_eddy} \\ R_{ss} = R_{ss\_ac} + R_{ss\_eddy} \end{cases}. \tag{6}$$

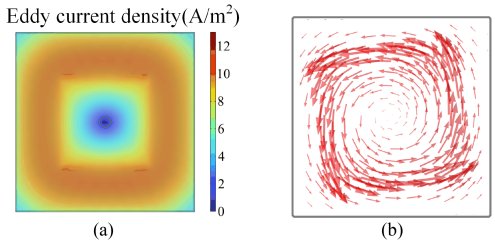

Fig. 8. Eddy current loss distribution of Q coil. (a) Eddy current density distribution of Qcoil. (b) Eddy current vector distribution of Q coil.

In the above equation, R_{sp_ac}(R_{ss_ac}) is the ac internal resistance introduced by L_{sp}(L_{ss}), and R_{sp_eddy}(R_{ss_eddy}) is the equivalent internal resistance due to eddy current loss generated by L_{sp}(L_{ss}) operating in seawater [11]. Fig. 8 shows the distribution of eddy current losses in the Q coil at $f_s = 8$ MHz for 0.01 A current excitation, which is mainly distributed at the four boundaries of the rectangle.

According to Fig. 2, it can be seen that the capacitive effect caused by the parasitic capacitance of the data coil during high-frequency signal excitation has an important influence on data transmission. Therefore, the parasitic capacitance C_{sp_pa} and C_{ss_pa} is considered in the steady-state model.

The coupled inductors L_{sp} and L_{ss} in Fig. 7(a) can be further equated to the T-equivalent circuit shown in Fig. 7(b). U_{in_signal} is the root mean square value of the power amplifier output signal u_{in_signal} with f_s and $\omega_s = 2\pi f_s$, $\omega_s^2 L_{sp} C_{sp} = \omega_s^2 L_{ss} C_{ss} = 1$. U_{out_signal} is the root mean square value of the voltage u_{out_signal} across the signal sampling resistor R_{signal}. Z_1, Z_2, and Z_3 are the equivalent input impedance of each port when looking in from left to right, respectively.

Data transfer gain G_s can be calculated that

$$G_s = \frac{U_{out\_signal}}{U_{in\_signal}} = G_{s1}G_{s2}G_{s3}G_{s4}. \tag{7}$$

Among them

$$\begin{cases} G_{s1} = \frac{Z_1}{Z_1 + 1/(j\omega_s C_{sp})} \\ G_{s2} = \frac{Z_2}{Z_2 + R_{sp} + j\omega_s(L_{sp} - M_s)} \\ G_{s3} = \frac{Z_3}{Z_3 + R_{ss} + j\omega_s(L_{ss} - M_s)} \\ G_{s4} = \frac{R_{signal}}{R_{signal} + 1/(j\omega_s C_{ss})} \end{cases} \tag{8}$$

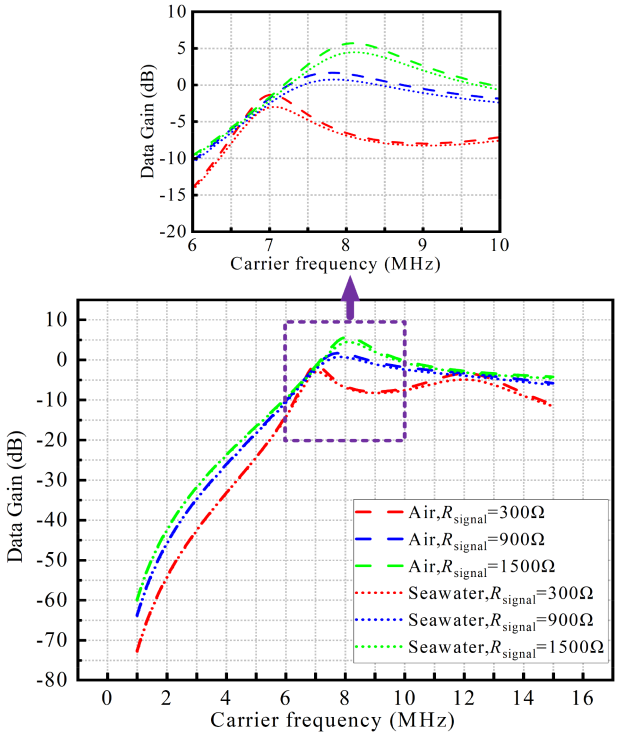

Fig. 9. Data gain at different R_{signal} in air and seawater.

and

$$\begin{cases} Z_1 = \dfrac{Z_2+R_{sp}+\mathrm{j}\omega_s(L_{sp}-M_s)}{\mathrm{j}\omega_s C_{sp\_pa}(Z_2+R_{sp}+\mathrm{j}\omega_s(L_{sp}-M_s))+1} \\ Z_2 = \dfrac{\mathrm{j}\omega_s M_s(Z_3+R_{ss}+\mathrm{j}\omega_s(L_{ss}-M_s))}{Z_3+R_{ss}+\mathrm{j}\omega_s L_{ss}} \\ Z_3 = \dfrac{\mathrm{j}\omega_s C_{ss} R_{\text{signal}}+1}{\mathrm{j}\omega_s(C_{ss}+C_{ss\_pa})-\omega_s^2 C_{ss} C_{ss\_pa} R_{\text{signal}}}. \end{cases} \tag{9}$$

Fig. 9 shows data gain at different R_{signal} in air and seawater, which involves the parameters shown in Table I. The center frequency of the carrier is set to 8 MHz. As R_{signal} increases, data gain increases both in air and in seawater. However, when R_{signal} is too low, the frequency corresponding to the maximum data gain point deviates from the set center frequency. For example, the frequency compared to the maximum data gain point at $R_{\text{signal}} = 900\ \Omega$ and $R_{\text{signal}} = 1500\ \Omega$ is close to 8 MHz. In contrast, the frequency corresponding to the maximum data gain point at $R_{\text{signal}} = 300\ \Omega$ is about 7 MHz. The frequency corresponding to the maximum data gain point gradually increases with the increase of R_{signal}. Compared with data gain in air, the trend of data gain in seawater is the same as in air, and the value decreases approximately 1 dB in the range of 7–9 MHz.

C. Data Transfer Dynamic Analysis

When the ASK is used for data transfer, the dynamic response process of the data is shown in Fig. 10. In Fig. 10, T_{s} is the time required to transfer one digital signature. T_{fall} is the transition time of the digital signature from "1" to "0," and T_{up} is the transition time of the digital signature from "0" to "1". T_{fall} and T_{up} determine the maximum communication rate.

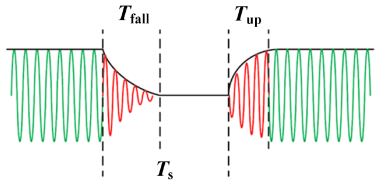

Fig. 10. Dynamic response process diagram of data.

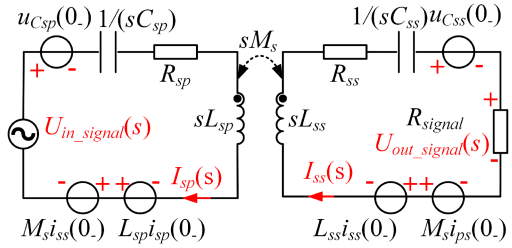

Fig. 11. Arithmetic circuit for SS compensation.

Since the equivalent circuit shown in Fig. 7(b) is a higher order system, it is simplified to the superposition of two second-order systems when the two parasitic capacitances of data coils are ignored to calculate the dynamic response process of the data. The simulation demonstrates that the accuracy of the DRT solution is essentially unaffected by such simplification. The Laplace transform is used to solve the dynamic response process. The arithmetic circuit is shown in Fig. 11.

In Fig. 11, $U_{\text{in\_signal}}(s)$ and $U_{\text{out\_signal}}(s)$ are the Laplace transform of $u_{\text{in\_signal}}(t)$ and $u_{\text{out\_signal}}(t)$, respectively. $I_{\text{sp}}(s)$ and $I_{\text{ss}}(s)$ are the Laplace transform of $i_{\text{sp}}(t)$ and $i_{\text{ss}}(t)$. $u_{\text{Csp}}(0_-)$ and $u_{\text{Css}}(0_-)$ are the voltage of C_{sp} and C_{ss} at the initial moment. $i_{\text{sp}}(0_-)$ and $i_{\text{ss}}(0_-)$ are the currents of L_{sp} and L_{ss} at the initial moment. Define the initial moment of the digital signature from "0" to "1" as $t = 0$. All energy storage components are fully discharged at $t = 0_-$, so $u_{\text{Csp}}(0_-) = u_{\text{Css}}(0_-) = 0$, $i_{\text{sp}}(0_-) = i_{\text{ss}}(0_-) = 0$. According to the KVL law, it is known that

$$\begin{cases} \left(1/\left(sC_{sp}\right) + sL_{sp} + R_{sp}\right) I_{sp} - sM_s I_{ss} = U_{in\_signal}(s) \\ \left(1/\left(sC_{ss}\right) + sL_{ss} + R_{ss}\right) I_{ss} - sM_s I_{sp} = 0. \end{cases} \tag{10}$$

Solving (10), it can be obtained

$$G_{up}(s) = \frac{U_{\text{out\_signal}}(s)}{U_{\text{in\_signal}}(s)} = \frac{Bs^3}{s^4 + A_0 s^3 + A_1 s^2 + A_2 s + A_3}. \tag{11}$$

Among them

$$\begin{cases} A_0 = \omega_s\left(1/Q_p + 1/Q_s\right)/\left(1/k_{\text{signal}}^2\right) \\ A_1 = \omega_s^2\left(2 + 1/\left(Q_p Q_s\right)\right)/\left(1 - k_{\text{signal}}^2\right) \\ A_2 = \omega_s^3\left(1/Q_p + 1/Q_s\right)/\left(1 - k_{\text{signal}}^2\right) \\ A_3 = \omega_s^4/\left(1 - k_{\text{signal}}^2\right) \\ B = \omega_s k_{\text{signal}}^2 R_{\text{signal}}/\left(\left(1 - k_{\text{signal}}^2\right)\omega_s M_s\right). \end{cases} \tag{12}$$

In (12), $Q_{\text{p}} = \omega_{\text{s}} L_{\text{sp}}/R_{\text{sp}}$, $Q_{\text{s}} = \omega_{\text{s}} L_{\text{ss}}/(R_{\text{ss}}+R_{\text{signal}})$. From (10)–(12), $u_{\text{out\_signal}}(t)$ is the zero-state sinusoidal response of a fourth-order system $G_{\text{up}}(s)$. To explore the relationship between the coefficients A_0–A_3, B and the DRT related to the circuit parameters, $G_{\text{up}}(s)$ can be decomposed into two second-order

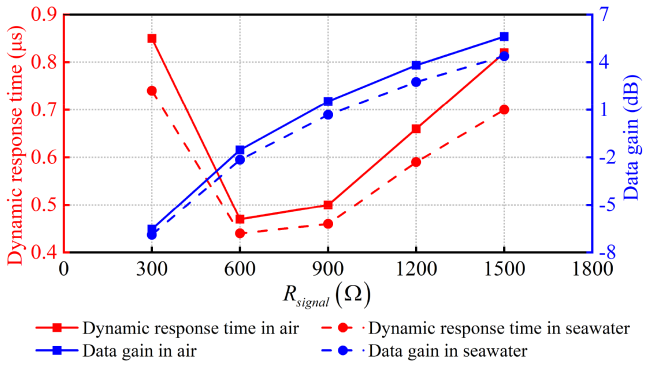

Fig. 12. Effect of R_{signal} on DRT and data gain.

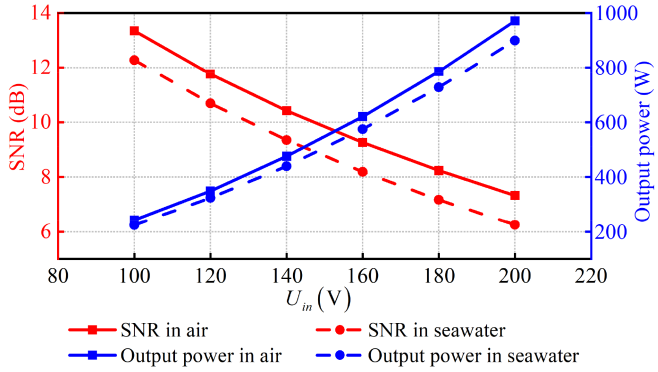

Fig. 13. Variation trends of SNR and output power in air and seawater.

systems

$$G_{\text{up}}(s) = G_{\text{up\_1}}(s) + G_{\text{up\_2}}(s) = \frac{K_1(s+z_1)}{s^2+2\xi_1\omega_{n1}s+\omega_{n1}^2} + \frac{K_2(s+z_2)}{s^2+2\xi_2\omega_{n2}s+\omega_{n2}^2}. \tag{13}$$

The partial coefficients in (13) meet the following conditions:

$$\begin{cases} A_0 = 2\xi_1\omega_{n1} + 2\xi_2\omega_{n2} \\ A_1 = \omega_{n1}^2 + \omega_{n2}^2 + 4\xi_1\xi_2\omega_{n1}\omega_{n2} \\ A_2 = 2\xi_1\omega_{n1}\omega_{n2}^2 + 2\xi_2\omega_{n2}\omega_{n1}^2 \\ A_3 = \omega_{n1}^2\omega_{n2}^2. \end{cases} \tag{14}$$

The time domain expression of $u_{\text{out\_signal}}$ is

$$u_{\text{out\_signal}}(t) = \mathcal{L}^{-1}\left[\left(G_{\text{up\_1}}(s) + G_{\text{up\_2}}(s)\right) U_{\text{in\_signal}}(s)\right]. \tag{15}$$

To obtain a fast dynamic response process, the communication system is usually set to an underdamped state, where the adjustment time required for $u_{\text{out\_signal}}$ to reach 95% of the steady-state value is

$$T_{\text{up}} = \max\{3/(\xi_1\omega_{n1}), 3/(\xi_2\omega_{n2})\}. \tag{16}$$

The detailed mathematical analysis shows that T_{fall} and T_{up} are equal. The solution procedure of T_{fall} is not derived in this article. Based on the abovementioned analysis, the maximum rate of data transfer is

$$v_{\max} = \frac{1}{\max\{3/(\xi_1\omega_{n1}), 3/(\xi_2\omega_{n2})\}}. \tag{17}$$

From (12)–(17), it is clear that increasing ω_{s} and k_{signal}, decreasing Q_{p} and Q_{s}, can raise A_0–A_3, thus increasing ξ_1, ξ_2, ω_{n1}, ω_{n2}, to obtain a smaller DRT and make the data reach the steady state quickly.

Fig. 12 shows that when R_{signal} increases, DRT decreases and then increases while data gain increases. When $R_{\text{signal}} =$ 600–900 Ω, DRT is less than 0.5 μs, but the corresponding data gain is not large. Moreover, because R_{sp} and R_{ss} in seawater are larger than in air, Q_{p} and Q_{s} in seawater are smaller when R_{signal} is constant, resulting in a smaller DRT in seawater than in air for the same parameters. Although lower Q_{p} and Q_{s} can somewhat reduce the DRT, they will result in relatively lower data gain. During the system design process, the constraint relationship between data gain and DRT should be sufficiently considered to find better circuit parameters to meet the system's performance requirements.

D. Crosstalk Analysis

Although the magnetic coupling structure proposed in this article is theoretically decoupled between power coils and data coils, it can lead to weak cross-coupling generation due to errors during experiments and other reasons. This coupling part cannot be neglected when performing a high-power transfer. Nevertheless, due to the band-pass filtering characteristics of the SS compensation network, low-frequency interference at frequency f_{p} during power transmission is greatly attenuated when coupled to the data circuit. Therefore, this part of the interference has basically no effect on the SWPDT system proposed in this article. However, the SS compensation network fails to show its bandpass filtering characteristics for EMI generated by the inverter, so it is the main source of interfering data. Regrettably, complex EMI models from the inverter cannot be accurately modeled. Accordingly, SNR is analyzed using the experimental results obtained from the experiments in this article.

Through extensive experiments, it was found that EMI generated by inverter can be estimated by the following equation:

$$G_{\text{noise}} = \frac{U_{\text{noise}}}{U_{\text{in}}} \approx 0.05. \tag{18}$$

Among the above, U_{noise} is EMI noise, which indicates the peak value of the noise detected on R_{signal} at the moment of inverter switching. SNR can be expressed as

$$\text{SNR} = \left|\frac{U_{\text{in\_signal}}G_s}{U_{\text{in}}G_{\text{noise}}}\right|. \tag{19}$$

Fig. 13 gives variation trends of SNR and output power at different U_{in} in air and seawater. With the increase of U_{in}, output power gradually increases while SNR is gradually decreasing. Meanwhile, SNR and output power trends are the same in air and seawater, while SNR and output power in seawater are smaller than in air. When the output power is 884 W in seawater, SNR is about 6 dB.

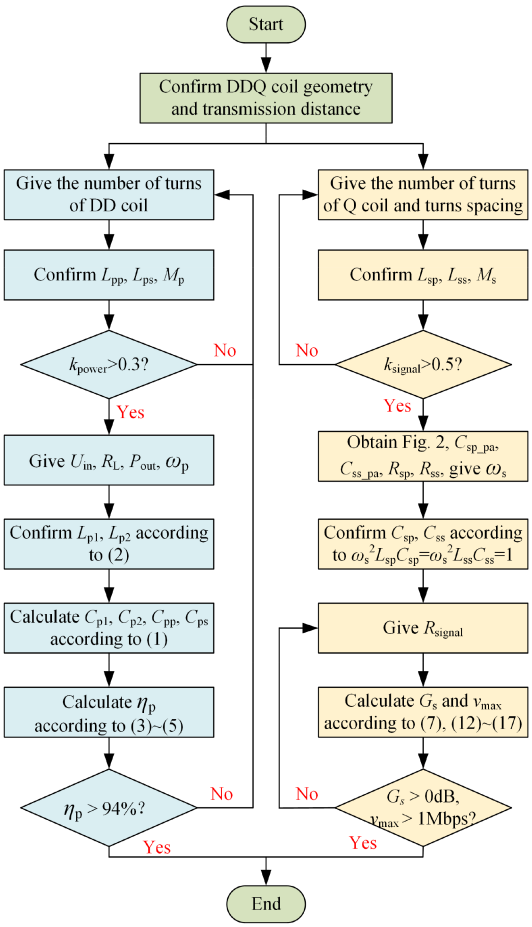

Fig. 14. Flowchart of system parameters design.

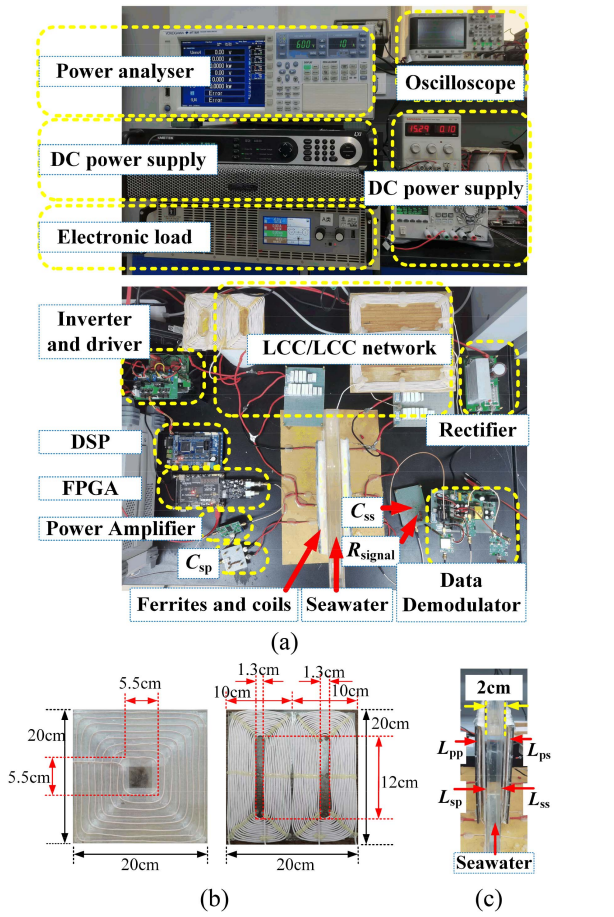

Fig. 15. Prototype proposed in this article. (a) Experimental platform of the prototype. (b) Geometry of the DDQ coil. (c) Front view of the magnetic coupling mechanism.

E. Procedure of Parametric Design

For the USWPDT system proposed in this article, WPT system and the communication system are decoupled, so the parameters of the system can be designed separately. The flowchart of system parameters design is shown in Fig. 14.

First, the geometrical constraints of the DDQ coil and the transmission distance of the system should be confirmed.

Second, the parameters of WPT system and communication system can be designed, respectively. For WPT system, the number of turns of the DD coil is given in this section by using a dense winding method from the outside to the inside. Then, L_{pp}, L_{ps}, and M_p can be obtained by finite element simulation. Two constraints for k_{power} greater than 0.3 and η_p greater than 94% are set, and the other parameters of WPT system can be calculated iteratively until the requirements are satisfying. For the communication system, the number of turns and turns spacing of the Q coil should be given in this section. Then, L_{sp}, L_{ss}, and M_s can be obtained by finite element simulation. According to the conclusion obtained from (17), k_{signal} needs to be maximized as a way to increase the communication rate. This article sets k_{signal} greater than 0.5. Next, the frequency characteristics of the Q coil are analyzed to give ω_s, C_{sp}, and C_{ss}. Based on the condition that G_s is greater than 0 dB and v_{max} is greater than 1 Mb/s, R_{signal} is obtained iteratively to meet the requirements.

Finally, circuit simulation is used to verify the parameters to meet the design requirements before building the prototype.

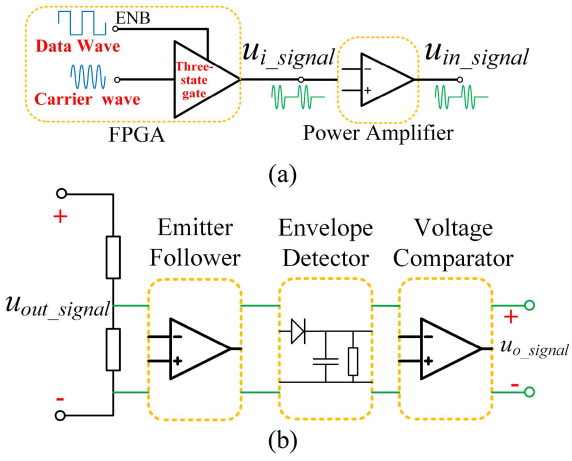

Fig. 16. Data modulation and demodulation circuit. (a) Data modulation circuit. (b) Data demodulation circuit.

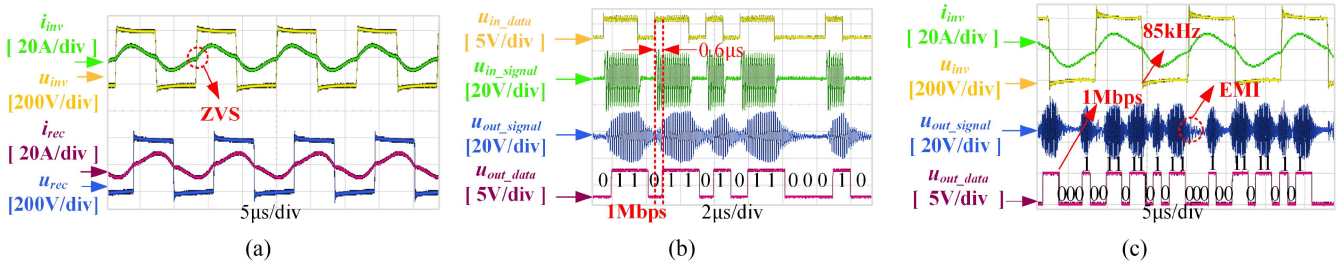

Fig. 17. Operating waveforms of the prototype. (a) Operating waveforms of inverter and rectifier in seawater. (b) Data waveform when there is no power transfer in seawater. (c) Operating waveforms during simultaneous power and data transfer in seawater.

Fig. 18. Maximum power point measured by the power analyzer.

IV. Experimental Verification

A. Experiment Setup

To verify the feasibility of the USWPDT system proposed in this article, a prototype with 884 W power transfer and 1 Mb/s data rate in seawater was built, as shown in Fig. 15(a). The geometry of the DDQ coil is given in Fig. 15(b), and the front view of the magnetic coupling mechanism is shown in Fig. 15(c).

For power transfer, SiC MOSFET(C3M0065090D) is selected in the inverter, and the diode(STTH100W04CW) is chosen in the rectifier. DSP28335 was selected as the controller. For data transfer, the ASK data modulation and demodulation circuit are shown in Fig. 16. The three-state gate circuit in FPGA generates the modulating signal $u_{\mathrm{i\_signal}}$ and output $u_{\mathrm{in\_signal}}$ after power amplifier to drive the SS compensation network. FPGA and power amplifier forms the ASK data modulation circuit, as shown in Fig. 16(a). The received data $u_{\mathrm{out\_signal}}$ is divided by the power resistor. Then, the demodulated data $u_{\mathrm{o\_signal}}$ is output through the emitter following circuit, envelope detector circuit, and threshold comparison circuit, respectively, which form the ASK data demodulation circuit, as shown in Fig. 16(b). The parameters of the prototype in seawater are given in Table I.

B. Experimental Results and Discussion

The experimental waveforms of the prototype are shown in Fig. 17. For power transfer, the operating waveforms of the inverter and rectifier at the maximum power point in seawater are given in Fig. 17(a). Fig. 18 shows the maximum power point measured by the power analyzer. At this point, the input power and output power are 937 W and 884 W, respectively. The transfer efficiency is 94.3%. The inverter achieves the ZVS condition, and the input impedance of the rectifier presents low inductance.

For data transfer, when there is no power transfer, the operating waveforms of data in seawater are given in Fig. 17(b). A random sequence "0110110101100010" is transferred as data. 1 bit of the random sequence is held for 1 μs, which means the data communication rate is 1 Mb/s. As can be seen in Fig. 17(b), the delay time between $u_{\mathrm{in\_data}}$ and $u_{\mathrm{out\_data}}$ is only 0.6 μs. Fig. 17(c) presents the operating waveforms when the power and data are transferred in seawater simultaneously. The frequency of u_{inv} and i_{inv} is 85 kHz, and the data communication rate is 1 Mb/s. The waveform of $u_{\mathrm{out\_signal}}$ presents EMI interference at the switch position. EMI interference value satisfies (19).

The eye diagram of the communication system is shown in Fig. 19. The reliability and interference characteristics of the communication system can be seen in the eye diagram. Fig. 19(a)–(c) show the eye diagrams measured at $U_{\mathrm{in}} = 0$ V, $U_{\mathrm{in}} = 100$ V, and $U_{\mathrm{in}} = 200$ V, respectively. From the abovementioned three-eye diagrams, it can be seen that the communication system is influenced by the greater EMI from WPT system as U_{in} increases. The eye height in the eye diagram is getting smaller and the line trace is getting wider, which means the noise is getting higher.

Fig. 20(a) and (b) compare theoretical and experimental values for output power and transfer efficiency in air and seawater when R_{L} is between 16 Ω and 36 Ω. The experimental and theoretical results are consistent with each other. It is noted that the theoretical values of the transfer efficiency in air and seawater are larger than the experimental values due to the measurement errors of the parameters in the experiment, the sensitivity of the experimental apparatus, and other reasons.

Fig. 21(a) and (b) compare theoretical and experimental values for data gain and DRT in air and seawater when R_{signal} is between 300 Ω and 1500 Ω. Data gain increases with R_{signal}. DRT is decreasing and then increasing with R_{signal}. Combining the data gain and DRT, an optimized R_{signal} can be obtained. The theoretical and experimental values are basically consistent.

Table II shows a comparison of some typical SWPDT systems. This article uses the ASK modulation method to transfer power 978 W in air and 884 W in seawater while achieving a data transfer rate 1 Mb/s. The power transfer efficiency reaches 94.6% and 94.3%, respectively. Reducing the parasitic capacitance of the data coil, EMI interference from the inverter, and optimizing the parameters of the data channel are effective ways to increase the data transfer rate in future research.

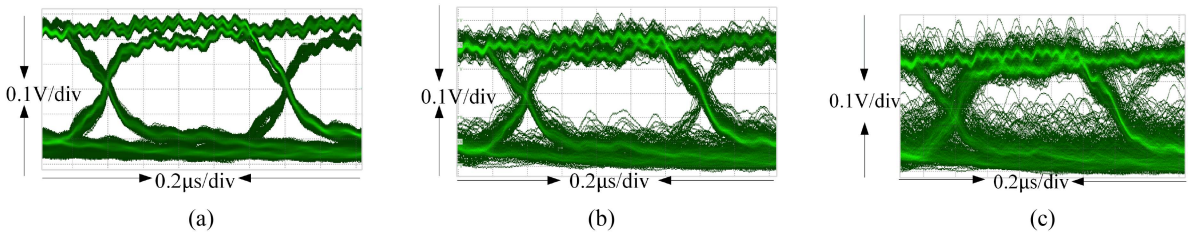

Fig. 19. Eye diagrams of the prototype. (a) $U_{\rm in} = 0$ V. (b) $U_{\rm in} = 100$ V. (c) $U_{\rm in} = 200$ V.

TABLE II
COMPARISON OF EXISTING WORKS AND THE PROPOSED SYSTEM

Reference	This article	[13]	[16]	[21]	[22]	[23]	[25]	[27]
Output Power	884 W	-	518 W	290 W	300 W	354 W	600 W	200 W
Transfer efficiency	94.3%	60%	92%	90%	90.1%	51.97%	85%	92.25%
Transfer medium	Seawater	Seawater	Seawater	Air	Air	Air	Air	Seawater
Transfer distance	2 cm	10 cm	3 cm	3 cm	6 cm	100 cm	5 cm	5 cm
Power working frequency	85 kHz	200 kHz	85 kHz	85 kHz	85 kHz	148 kHz	85 kHz	249.2 kHz
Carrier wave frequency	8 MHz	2 MHz/10 MHz	5.4 MHz/7.3 MHz	1 MHz	4.5 MHz/5.5 MHz	2.5 MHz	2 MHz/1.2 MHz	1.5 MHz
Data rate	1 Mb/s	2 kb/s	700 kb/s	166.7 kb/s	500kb/s	19.2 kb/s	80 kb/s	30 kb/s
Modulation method	ASK	FSK	FSK	ASK	FSK	ASK	ASK	ASK
Analyze DRT	Yes	No	No	Yes	No	No	No	No
Coupling mechanism	DDQ	Single coil	The last turn	DD	Coil taps	Single coil	Single coil	Single coil
Coil size/cm	20×20	-	Φ30×20	15×15	Φ19.5	85×85	-	-

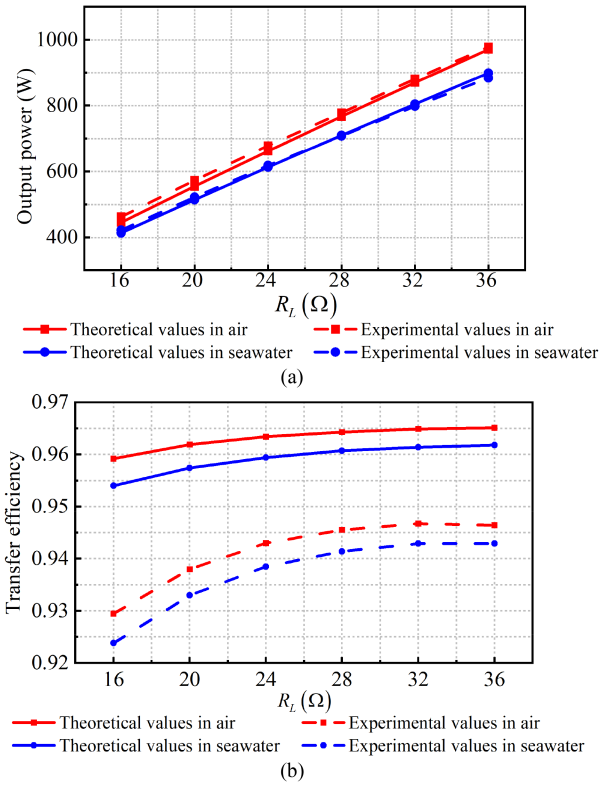

Fig. 20. Comparison of power transfer characteristics. (a) Comparison of theoretical and experimental output power. (b) Comparison of theoretical and experimental transfer efficiency.

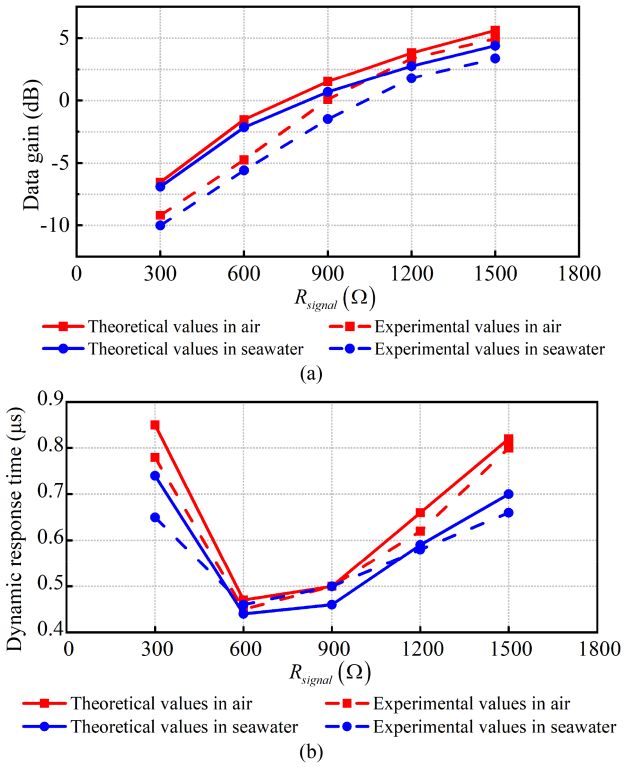

Fig. 21. Comparison of data transfer characteristics. (a) Comparison of theoretical and experimental data gain. (b) Comparison of theoretical and experimental DRT.

V. Conclusion

This article proposes a USWPDT system based on DDQ coil, which can achieve a 1 Mb/s communication rate. Considering the parasitic capacitance and DRT of the data channel as essential factors limiting the communication rate, data gain, and DRT are accurately calculated and analyzed in air and seawater by the steady state and dynamic models of the data channel. Due to the attenuation characteristics of high-frequency electromagnetic waves in seawater, eddy current loss affects not only the transfer power and efficiency but also the data gain and SNR. This article presents a detailed theoretical analysis and experimental verification of influence tendency. Finally, a prototype achieves 884 W power transfer and 1 Mb/s communication rate in seawater. The results of this article contribute to the application of SWPDT systems on AUV. Future research will focus on Mb/s-class USWPDT system in full duplex mode.

References

[1] Z. Liu, L. Wang, Y. Guo, and S. Li, "Primary-side linear control for constant current/voltage charging of the wireless power transfer system based on the LCC-N compensation topology," *IEEE Trans. Ind. Electron.*, vol. 69, no. 9, pp. 8895–8904, Sep. 2022.

[2] C.-C. Huang, C.-L. Lin, and Y.-K. Wu, "Simultaneous wireless power/data transfer for electric vehicle charging," *IEEE Trans. Ind. Electron.*, vol. 64, no. 1, pp. 682–690, Jan. 2017.

[3] Y. Guo, Y. Zhang, S. Li, C. Tao, and L. Wang, "Load parameter joint identification of wireless power transfer system based on the DC input current and phase-shift angle," *IEEE Trans. Power Electron.*, vol. 35, no. 10, pp. 10542–10553, Oct. 2020.

[4] T. Wang, Q. Xu, W. Jia, Z.-H. Mao, H. Tang, and M. Sun, "Dual-functional wireless power transfer and data communication design for micromedical implants," *IEEE J. Emerg. Sel. Topics Power Electron.*, vol. 9, no. 5, pp. 6259–6271, Oct. 2021.

[5] L. Wang, X. Li, S. Raju, and C. P. Yue, "Simultaneous magnetic resonance wireless power and high-speed data transfer system with cascaded equalizer for variable channel compensation," *IEEE Trans. Power Electron.*, vol. 34, no. 12, pp. 11594–11604, Dec. 2019.

[6] J. Zhou, D. Li, and Y. Chen, " Frequency selection of an inductive contactless power transmission system for ocean observing," *Ocean Eng.*, vol. 60, pp. 175–185, Jan. 2013.

[7] Y. Yao, P. Sun, X. Liu, Y. Wang, and D. Xu, "Simultaneous wireless power and data transfer: A comprehensive review," *IEEE Trans. Power Electron.*, vol. 37, no. 3, pp. 3650–3667, Mar. 2022.

[8] P. Guo, R. Yuan, C. Cai, H. Lin, and L. Yang, "High-data-frequency-ratio information transmission method for fast dynamic response SWPIT systems based on DASK modulation," *IEEE J. Emerg. Sel. Topics Power Electron.*, vol. 9, no. 3, pp. 3822–3834, Jun. 2021.

[9] T. Kan, R. Mai, P. P. Mercier, and C. C. Mi, "Design and analysis of a three-phase wireless charging system for lightweight autonomous underwater vehicles," *IEEE Trans. Power Electron.*, vol. 33, no. 8, pp. 6622–6632, Aug. 2018.

[10] D. Wang, S. Cui, J. Zhang, Z. Bie, K. Song, and C. Zhu, "A novel arc-shaped lightweight magnetic coupler for AUV wireless power transfer," *IEEE Trans. Ind. Appl.*, vol. 58, no. 1, pp. 1315–1329, Jan./Feb. 2022.

[11] Z. Liu, L. Wang, Y. Guo, and C. Tao, "Eddy current loss analysis of wireless power transfer system for autonomous underwater vehicles," in *Proc. IEEE PELS Workshop Emerg. Technol., Wireless Power Transfer*, 2020, pp. 283–287.

[12] Z. Yan et al., "Frequency optimization of a loosely coupled underwater wireless power transfer system considering eddy current loss," *IEEE Trans. Ind. Electron.*, vol. 66, no. 5, pp. 3468–3476, May 2019.

[13] L. Yang et al., "Undersea wireless power and data transfer system with shared channel powered by marine renewable energy system," *IEEE Trans. Emerg. Sel. Topics Circuits Syst.*, vol. 12, no. 1, pp. 242–250, Mar. 2022.

[14] R. Naghash, S. M. M. Alavi, and S. E. Afjei, "Robust control of wireless power transfer despite load and data communications uncertainties," *IEEE J. Emerg. Sel. Topics Power Electron.*, vol. 9, no. 4, pp. 4897–4905, Aug. 2021.

[15] C.-C. Huang and C.-L. Lin, "Wireless power and bidirectional data transfer scheme for battery charger," *IEEE Trans. Power Electron.*, vol. 33, no. 6, pp. 4679–4689, Jun. 2018.

[16] Y. Wang, T. Li, M. Zeng, J. Mai, P. Gu, and D. Xu, "An underwater simultaneous wireless power and data transfer system for AUV with high-rate full-duplex communication," *IEEE Trans. Power Electron.*, vol. 38, no. 1, pp. 619–633, Jan. 2023.

[17] J. Oiler, G. Anderson, V. Bana, A. Phipps, M. Kerber, and J. D. Rockway, "Thermal and biofouling effects on underwater wireless power transfer," in *Proc. IEEE Wireless Power Transfer Conf.*, 2015, pp. 1–4.

[18] M. M. Ahmadi, S. Pezeshkpour, and Z. Kabirkhoo, "A high-efficiency ASK-modulated class-E power and data transmitter for medical implants," *IEEE Trans. Power Electron.*, vol. 37, no. 1, pp. 1090–1101, Jan. 2022.

[19] X. Li, C. Tang, X. Dai, P. Deng, and Y. Su, "An inductive and capacitive combined parallel transmission of power and data for wireless power transfer systems," *IEEE Trans. Power Electron.*, vol. 33, no. 6, pp. 4980–4991, Jun. 2018.

[20] X. Li, J. Hu, Y. Li, H. Wang, M. Liu, and P. Deng, "A decoupled power and data-parallel transmission method with four-quadrant misalignment tolerance for wireless power transfer systems," *IEEE Trans. Power Electron.*, vol. 34, no. 12, pp. 11531–11535, Dec. 2019.

[21] G. Wei, J. Feng, J. Zhang, C. Wang, C. Zhu, and S. Y. Ostanin, "An efficient power and data synchronous transfer method for wireless power transfer system using double-D coupling coil," *IEEE Trans. Ind. Electron.*, vol. 68, no. 11, pp. 10643–10653, Nov. 2021.

[22] Y. Yao, H. Cheng, Y. Wang, J. Mai, K. Lu, and D. Xu, "An FDM-based simultaneous wireless power and data transfer system functioning with high-rate full-duplex communication," *IEEE Trans. Ind. Inform.*, vol. 16, no. 10, pp. 6370–6381, Oct. 2020.

[23] L. Ji, L. Wang, C. Liao, and S. Li, "Simultaneous wireless power and bidirectional information transmission with a single-coil, dual-resonant structure," *IEEE Trans. Ind. Electron.*, vol. 66, no. 5, pp. 4013–4022, May 2019.

[24] P. Wang, Y. Sun, T. Feng, Y. Fan, and Y. Feng, "Simultaneous wireless power and data transfer system with full-duplex mode based on double-side LCCL and dual-notch filter," *IEEE J. Emerg. Sel. Topics Power Electron.*, vol. 10, no. 3, pp. 3140–3151, Jun. 2022.

[25] Y. Fan, Y. Sun, X. Dai, Z. Zuo, and A. You, "Simultaneous wireless power transfer and full-duplex communication with a single coupling interface," *IEEE Trans. Power Electron.*, vol. 36, no. 6, pp. 6313–6322, Jun. 2021.

[26] Y. Yao et al., "Analysis and design of a simultaneous wireless power and data transfer system featuring high data rate and signal-to-noise ratio," *IEEE Trans. Ind. Electron.*, vol. 68, no. 11, pp. 10761–10771, Nov. 2021.

[27] Y. Zeng, C. Lu, R. Liu, X. He, C. Rong, and M. Liu, "Wireless power and data transfer system using multidirectional magnetic coupler for swarm AUVs," *IEEE Trans. Power Electron.*, vol. 38, no. 2, pp. 1440–1444, Feb. 2023.

Chaolai Da received the B.S. degree in electrical engineering and its automation from Hebei University of Technology, Tianjin, China, in 2021. He is currently working toward the Ph.D. degree in electrical engineering with the Institute of Electrical Engineering, Chinese Academy of Sciences, Beijing, China.

His research interests include undersea wireless power transfer and simultaneous wireless power and data transfer.

Lifang Wang (Member, IEEE) received the Ph.D. degree in automotive engineering from Jilin University, Jilin, China, in 1997.

She was with the Institute of Electrical Engineering, Chinese Academy of Sciences (IEECAS), Beijing, China. During the Chinese tenth-five year plan (2001–2005), she was a member of the national specialist group of Key Special Electric Vehicle Project of the National 863 Program, and she was the Head of the 863 Special EV Project Office. She is currently the Director of the Department of Vehicle Energy System and Control Technology, IEECAS. She is also the Vice Director of the Key Laboratory of Power Electronics and Electric Drives, Chinese Academy of Sciences. Her research interests include wireless charging system for EV, EV control system, EV battery management system, electromagnetic compatibility, and smart electricity use.

Fang Li received the Ph.D. degree is electrical engineering from the Institute of Electrical Engineering, Chinese Academy of Sciences, Beijing, China, in 2009.

She is currently an Associate Professor with the Department of Vehicle Energy System and Control Technology, Institute of Electrical Engineering. Her research interests include wireless power transmission, simultaneous wireless information and power transfer, and intelligent vehicle control.

Chengxuan Tao (Member, IEEE) received the M.S. degree in control science and engineering from Chongqing University, Chongqing, China, in 2012. He is currently working toward the Ph.D. degree in mechanical engineering with the Beijing Institute of Technology, Beijing, China.

He is currently a Senior Engineer with the Key Laboratory of Power Electronics and Electric Drives, Chinese Academy of Sciences. His research interests include circuit topology, analysis and control of wireless power transfer system, especially its applications in special fields.

Yuwang Zhang received the M.S. degree in electronic science and technology from the Wuhan University of Technology, Wuhan, China, in 2015, and the Ph.D. degree in electrical engineering from the Institute of Electrical Engineering, Chinese Academy of Sciences (IEECAS), Beijing, China, in 2020.

He is currently a Postdoctoral with the Department of Vehicle Energy System and Control Technology, IEECAS. His research interests include wireless power transfer theory, optimization and control of electric vehicle wireless charging system, and bidirectional wireless charging system.